J Mater Sci: Mater Med (2008) 19:451–457
DOI 10.1007/s10856-006-0052-7

Titanium scaffolds for osteointegration: mechanical, in vitro and corrosion behaviour

Sandra C. P. Cachinho · Rui N. Correia

Received: 7 August 2006 / Accepted: 20 November 2006 / Published online: 3 July 2007

Abstract While titanium has been successful as an orthopaedic or dental implant material, performance problems still persist concerning implant-bone interfacial strength and mechanical modulus mismatch between metal and tissue. Porous structures are an advantageous alternative because the elastic modulus can be adjusted to match that of bone, thereby preventing bone resorption. Furthermore, to achieve early and strong stabilization theses structures may be coated with bioactive deposits, as hydroxyapatite. In the present work, titanium porous scaffolds were produced from TiH_2 slurry by a replication sponge reactive sintering method, and coated with hydroxyapatite by the sol-gel process. The obtained structures were microstructurally and mechanically characterized. Their in vitro bioactivity was investigated by soaking in a simulated body fluid (SBF). Electrochemical characterization was also performed in order to evaluate the effect of coating on corrosion resistance.

The scaffolds exhibit a three-dimensionally interconnected porous structure that can be mechanically and morphologically compared to trabecular bone. Their in vitro bioactivity suggests potential for osseous integration. Coating also improves corrosion resistance in physiologically saline environment.

S. C. P. Cachinho (✉) · R. N. Correia
Department of Ceramics and Glass Engineering,
University of Aveiro, 3810-193 Aveiro, Portugal
e-mail: scachinho@cv.ua.pt

Introduction

Titanium has been used extensively for skeletal repair and dental implants. There are, however, unsolved technical problems associated with the use of titanium as an implant material. The bioinert character of its protective naturally forming surface oxide does not readily form a strong interface with surrounding tissue. Furthermore, the relatively high stiffness of titanium, as compared to surrounding bone, can lead to problems of stress-shielding and subsequent implant loosening [1]. So, the mismatch of Young's modulus between bone (10–30 GPa) and bulk metallic materials (between 110 GPa for Ti and 230 GPa for Co–Cr alloys) has been identified as the main reason for implant loosening [2].

To address these issues, current attempts in implant design have shifted towards the development of biomaterials incorporating three-dimensional osteocondutive scaffolds for bone regeneration [3]. The advantage of porous materials is their ability to provide biological anchorage for the surrounding bony tissue via ingrowth of mineralized tissue into the pore space [4]. Besides, their elastic moduli can be adjusted to match that of trabecular bone, thereby limiting stress shielding and preventing bone resorption at the implant interface [3].

In such circumstances the porous matrix must be designed to satisfy several requirements, namely that the material chosen must be biocompatible and bioactive [5] and that the porous structure must be designed with interconnected porosity providing sufficient space for cell migration, adhesion, proliferation and the ingrowth of new bone tissue [5, 6]. In this way, the optimal pore size for bone ingrowth will be between 100 and 500 μm [4].

To obtain structures with the proper pore size, morphology and interconnectivity, several kinds of methods

have been proposed, such as the use of organic additives, freeze-drying methods, powder metallurgy, polymeric sponge methods, and so on. Among them, polymeric foam replication might be one of the most effective methods to produce metallic scaffolds with interconnected pores because of its favourable structure, simple processing and cheapness [3, 6, 7].

The aim of the present work was to prepare and characterize in vitro bioactive and macroporous titanium scaffolds by the polymeric sponge method.

Experimental

Specimen preparation

Porous specimens were prepared by the sacrificed polymeric sponge method, from an optimized TiH_2 slurry containing 45 vol% TiH_2 powder, 0.3 wt% Dispex A40 and 0.07 wt% carrageenan in ultra-pure water. The powder, purchased from Aldrich with 98% purity, had a mean particle size of 15.6 μm and a specific surface area of 0.5336 m^2/g.

Polymeric sponge blocks were dipped into the slurry and infiltrated. After withdrawal the excess slurry was removed by gentle compression followed by drying at room temperature for 24 h. Removal of the sponge, hydride decomposition and sintering of the resulting titanium block to a porous scaffold were performed during a thermal cycle under high vacuum (10^{-6} mbar) and a low heating rate (1°C/min) with dwellings at 500°C (2 h) and 1,000°C (4 h).

For pore size evaluation and mechanical tests blocks were cut, polished (1200 grit) and ultrasonically sequentially cleaned in acetone and alcohol for 10 min.

Physical characterization

X-ray diffraction (XRD, Rigaku PMG-VH) using Cu K_α radiation was used to confirm the presence of titanium metal as the final product of the thermal treatment. The porous microstructures were observed by scanning electron microscopy (SEM, Hitachi S4100). Porosity (P) was determined on 10 samples by measuring their apparent geometrical density (ρ_a) and using the correspondence $P = 1-(\rho_a/\rho)$ where ρ is the metal density (4.5 g/cm^3). The mean pore size was assessed at low magnification (30×) in scanning electron microscopy (SEM). Compression tests were performed on 5 blocks of approximately $17 \times 8.4 \times 5.8$ mm^3 at a crosshead speed of 1 mm/min (Shimadzu Autograph AG-25TA). Compressive strains were calculated considering deformation as corresponding to the crosshead displacement and the Young's modulus was taken as the derivative of the linear portion of the stress-strain curve.

Sol-gel coating

Pore coating with hydroxyapatite (HA) was achieved by gelification of a mixture of calcium nitrate tetrahydrate, $Ca(NO_3)_2{\cdot}4H_2O$, and diethyl phosphite, $C_4H_{11}O_3P$, diluted in ultra-pure water and stirred for 2 h in air. Five layers were applied in successive cycles of infiltration of the porous scaffolds, consisting of immersion at 6 cm/min, dwelling in solution for 5 min, withdrawal and drying at 110°C in air, for 5 min.

After deposition of the final layer, samples were annealed at 700°C for 3 h in air and observed in SEM with energy dispersive spectroscopy (EDS) for morphological and chemical characterization of the deposits.

In vitro tests

Samples with $10 \times 10 \times 5$ mm^3 were immersed in 10 ml of tris-buffered Kokubo's simulated body fluid (SBF, Table 1) at initial pH of 7.24, inside polypropylene containers, at 37°C and under gentle shaking. Immersion times were 1, 3 and 7 days and samples were rinsed with distilled water and dried at the end of each period. Pore surface modifications during immersion were analyzed by SEM/EDS, while test solutions were characterized by inductively coupled plasma (ICP) spectroscopy to determine the evolution of ionic composition during immersion.

Electrochemical tests

The corrosion behaviour of coated and non-coated scaffolds in a physiologically saline environment was studied in a 0.9% wt/vol. NaCl aqueous solution at 37°C, open to air, with a Radiometer Analytical Voltalab 10 PGZ 100 source. Measurements were performed in a three-electrode cell consisting of the sample, a saturated calomel electrode as reference and a platinum electrode as cathode. Each

Table 1 Ionic composition of SBF and Human Blood Plasma ($mM.l^{-1}$)

	Na^+	K^+	Mg^{2+}	Ca^{2+}	Cl^-	HCO_3^-	HPO_4^{2-}	SO_4^{2-}
SBF	142.0	5.0	1.5	2.5	147.8	4.2	1.0	0.5
Plasma	142.0	5.0	1.5	2.5	103.0	27.0	1.0	0.5

block was varnished to leave an exposed area of 10×5 mm^2 to the electrolyte.

The open circuit potential was measured after the specimens were immersed in the solution for 30 min. The polarization resistance was measured in the –10 to +10 mV range. The polarization curves were recorded in the –1000 to +2000 mV range at a scanning rate of 1 mV/s. Two specimens were tested per test mode.

Results and discussion

Complete conversion of the hydride to titanium metal in sintered porous structures is confirmed by XRD (Fig. 1). Also, no titanium oxide traces are detected.

The sintered scaffolds (Fig. 2) present interconnected macropores, as required for cell colonization and vascularization [6]. Macropores are sized in the range of 100–600 μm and have rounded shapes, appropriate for the ingrowths of the new-bone tissues and the transport of the body fluids [5]. Micropores can also be observed at pore walls, presumably resulting from volume shrinkage during the reactive sintering process of the TiH_2 powders. The minimum value for the pore size obtained is in the lower limit usually considered for use in bone-integrating orthopaedic implants, while the maximum size slightly exceeds the reported value of 500 μm [4]. These values can obviously be adjusted by selecting sponges with different architectures. The trabeculae show a rough surface, a characteristic that may play an important role in the process of bone formation, because it is favourable for cell seeding, cell attachment, proliferation, differentiation and ingrowth of tissue [4]. Structures prepared by this method have approximately 75% porosity.

Figure 3 shows the compressive stress-strain curve of the scaffolds. After an accommodation stage it is possible

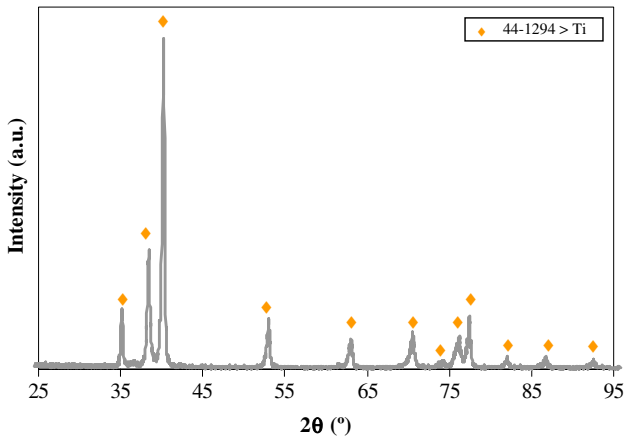

Fig. 1 XRD patterns of titanium scaffolds sintered at 1000°C

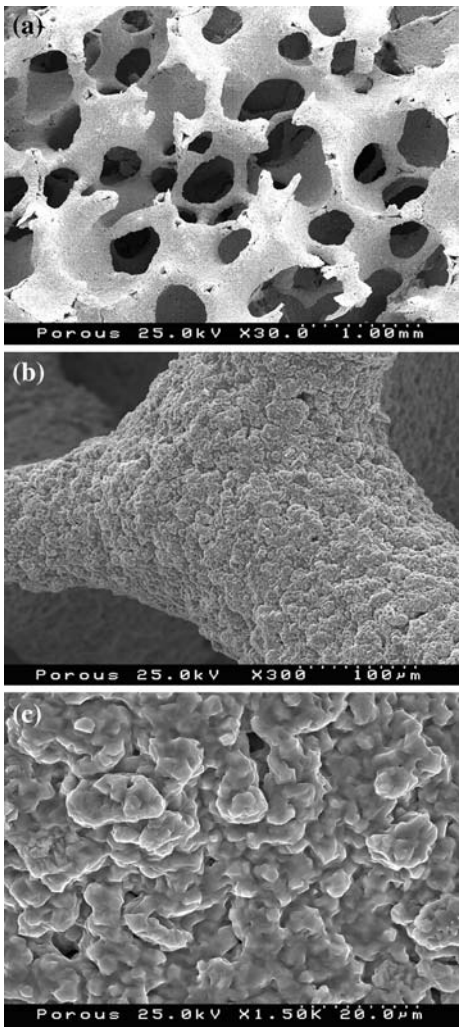

Fig. 2 SEM micrographs of the surface and microstructure porous titanium samples with different magnification: (**a**) 30×, (**b**) 300× and (**c**) 1.5 k×

to identify a linear response, followed by a stress oscillation corresponding to progressive pore wall collapse. Finally, there is a region (not totally shown) where a slow stress decrease leads to complete fracture. The compressive strength and Young's moduli were calculated for the linear part of the compressive stress-strain curve (Table 2) and the values obtained compare with those for stiffer trabecular bone tissue. The mismatch of Young's modulus between bone and bulk materials can thus be eliminated with the use of porous metallic structures. A proper choice of a different sponge structure should also allow the production of metallic structures to mimic cortical bone.

The selection of titanium for implants is related to its excellent biocompatibility, due to the spontaneous formation of an oxide layer in both air and physiological environment, which limits ion release [3]. Nevertheless, a hydroxyapatite coating enhances the bioactivity and os-

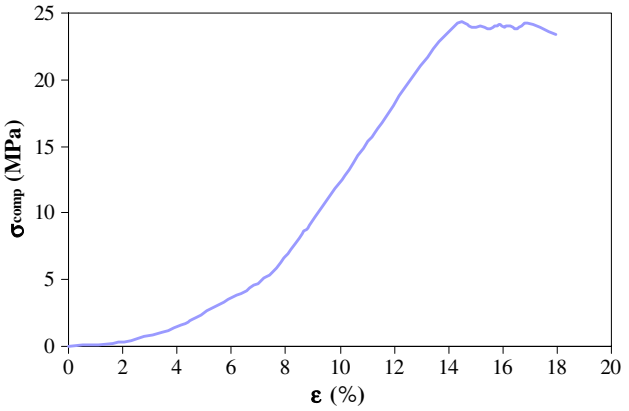

Fig. 3 Compressive stress-strain curve of titanium scaffolds

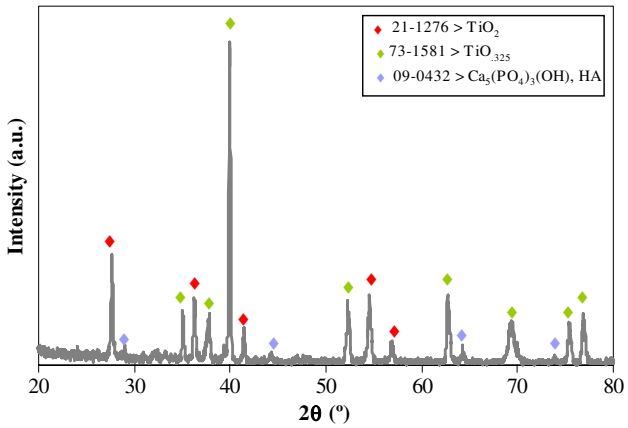

Fig. 4 XRD patterns of titanium scaffolds after coating with hydroxyapatite and heat treatment at 700°C for 3 h

Table 2 Compressive mechanical properties of the porous titanium scaffolds, bulk titanium and bone [8–13]

Materials	σ_{comp} (MPa)	E (GPa)
Scaffolds	23.72 ± 1.12	0.30 ± 0.003
Titanium	450–965	100–110
Cortical bone	80–120	3–30
Trabecular bone	2–12	0.05–0.5

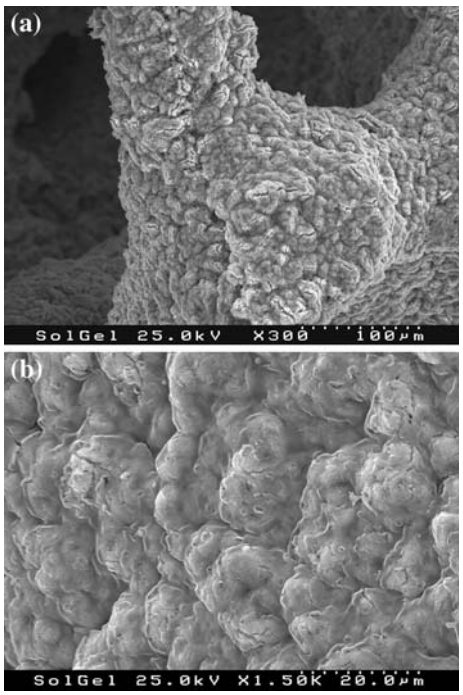

Fig. 5 SEM morphologies of hydroxyapatite coated scaffolds after heat treatment at 700°C for 3 h: (**a**) 300×, (**b**) 1.5 k×

teoconductivity during the initial stage following implantation, promoting osteoblast differentiation and proliferation [14]. It is also expected that the oxide titanium layer formed confers corrosion resistance to the titanium substrate, even after the HA layer is completely dissolved due to biological processes. In addition, the favourable chemical affinity of TiO_2 with respect to HA as well as to Ti contributes to the improvement of bonding strength between coating and substrate [15].

To improve the biological properties of titanium the porous structures were sol-gel coated with hydroxyapatite (HA). After heat treatment at 700°C, XRD revealed the presence of three phases, TiO_2, $TiO_{.325}$ and HA (Fig. 4). No significant changes in mechanical parameters could be found after heat treatment, so that oxidation is considered superficial. Figure 5 shows typical morphologies of the coated pores after heat treatment. Samples are uniformly coated and the film shows a granular structure. The same aspect was found by Lim et al. [16], after coating Ti-6Al-4V substrates by the sol-gel process. The coated surfaces were analysed by EDS, and found to be rich in calcium and phosphorous, with a Ca/P atom ratio of 1.61, near to the stoichiometric value for hydroxyapatite.

Figures 6, 7 and 8 describe the mineralization behaviour of uncoated and sol-gel HA-precoated titanium scaffolds during immersion in SBF. Uncoated scaffolds do not show mineralizing deposits after 7 days of immersion; in contrast, precoated specimens display morphological modifications that suggest mineralization after the same period (Fig. 6). These changes are already visible after 3 days, as can be seen in Fig. 6a–c. The Ca and P ion concentration time profiles in SBF (Fig. 8) indicate no changes for uncoated specimens, whereas in the precoats a dissolution process is dominant until 3 days, followed by a net deposition between 3 and 7 days. The dissolution stage corresponds to a preferential depletion of Ca in the coating (Fig. 7) down to 1.35—a value that may correspond to octacalcium phosphate—OCP ($Ca_8H_2(PO_4)_6{\cdot}5H_2O$, Ca/P = 1.33—but further deposition

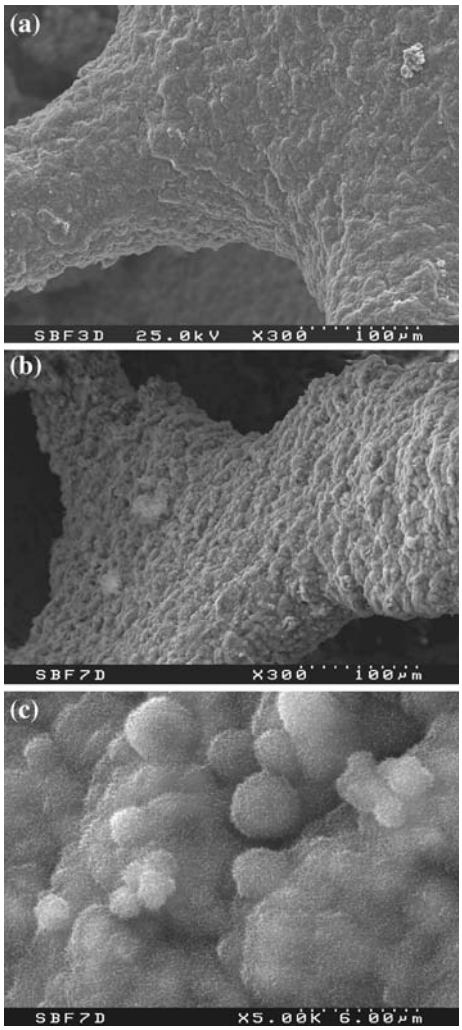

Fig. 6 SEM images of hydroxyapatite coated scaffolds after being immersed in SBF for: (**a**) 1 day, (**b**) 3 days and (**c**) 7 days

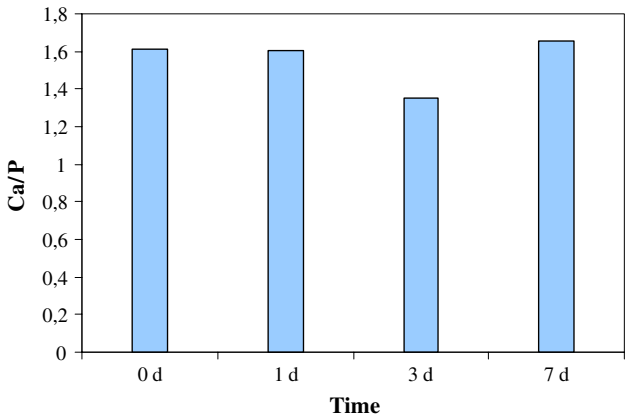

Fig. 7 EDS analysis of HA coated scaffolds soaked in SBF

leads to a recovery of the near-stoichiometric Ca/P ratio of hydroxyapatite. OCP is known as a precursor phase of hydroxyapatite in the mineralization process [17]. Extending

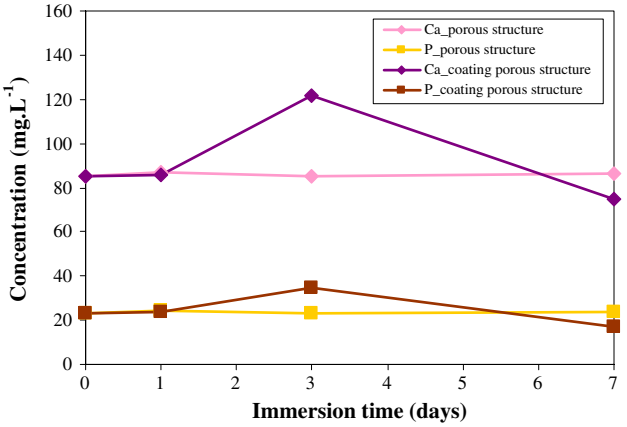

Fig. 8 Ca and P concentrations in SBF soaking solutions

the immersion period in SBF this phase would be expected to transform into hydroxyapatite by consuming calcium ions from the solution, according to:

$$Ca_8H_2(PO_4)_6 \cdot 5H_2O(s) + 2Ca^+(aq) \leftrightarrow Ca_{10}(PO_4)_6(OH)_2(s) + 3H_2O(l) + 4H^+(aq)$$

Thus, after 7 days an apatite layer on pore walls finally occurs (Fig. 6b) as spherical aggregates of acicular crystals, a typical hydroxyapatite morphology (Fig. 6c).

Coating the implant with a ceramic such as calcium phosphate can accelerate the formation of an apatite layer on its surface [18]. Amongst the materials employed, hydroxyapatite coatings are especially attractive, as a bone-like material is introduced in the interface between the metal and the living tissue. Moreover, the stability of these biomaterials stems from their electrochemical passivity, and their ability to avoid passivity breakdown in the highly aggressive physiological environment [19].

Materials contact in vivo with extracellular body fluids. The chloride ion concentration in blood plasma (113 $mEq.l^{-1}$) and in interstitial fluid (117 $mEq.l^{-1}$) is sufficiently high to corrode most metallic materials, so that the corrosion resistance of metallic biomaterials is a concern [20]. The metallic materials used as implants have a passive film that rapidly forms in the body fluid environment and confers corrosion resistance. However, the corrosion behaviour is also related to the electrolyte concentration and environmental conditions (e.g., pH, concentration of dissolved oxygen and temperature) [21]. If metallic materials are corroded by body fluids undesirable reactions can occur, such as toxicity and allergy, by release of metal ions into the body fluid for a prolonged period of time [20]. Since metallic materials used as chirurgical implants are not retrieved in many cases, either because of its obligatory presence or to avoid a second surgery, they

should have high corrosion resistance [22]. In fact, the in vitro evaluation of such parameter represents one of the first stages in the procedure to accept new materials for that purpose [20, 23].

The open circuit corrosion potential E_{oc} of the scaffolds in NaCl solution was recorded as a function of time, at 37°C, as shown in Fig. 9. After 30 min the potential stabilized at –52 mV for titanium, and –149 mV for HA-coated titanium, meaning that coating increases corrosion resistance. Polarization curves are depicted in Fig. 10. Table 3 shows average values of E_{oc}, together with the corrosion potential E_{corr}, corrosion current I_{corr} and polarization resistance per unit area R_p, determined from polarization tests.

As expected, the corrosion potentials determined from polarization curves are approximately equal to those obtained from open circuit potential measurements. The cathodic polarization regime in Fig. 10 denotes a passive behaviour of both types of scaffold, but more so for coated scaffolds. In the case of bare scaffolds this regime is related with the formation of an oxide film [23]. However, at potentials above corrosion potential the increase in current density suggests that this film is gradually destroyed or replaced by a less protective film. Irregularities in the anodic portion of the polarization curve for HA-coated scaffolds, apparently due to a more complex process, possibly implying the HA deposit. The shift of the polarization curve of the uncoated sample to higher values of current density shows a greater tendency to corrosion when compared with the coated sample [19]. The polarization resistance values in Table 3 corroborate the higher electrochemical inertness of HA-coated scaffolds. These results agree with previous findings that the corrosion resistance of titanium could be improved by Ca and P ion implantation [24, 25], like that of steel by sol-gel coating with calcium phosphate [26].

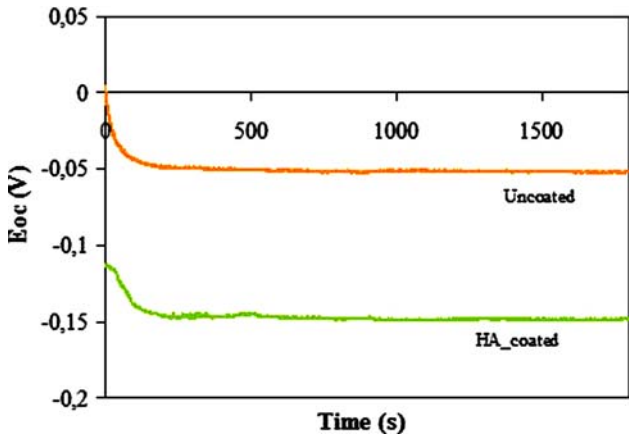

Fig. 9 Open-circuit corrosion potential vs. time curves for scaffolds in 0.9% NaCl solution at 37°C

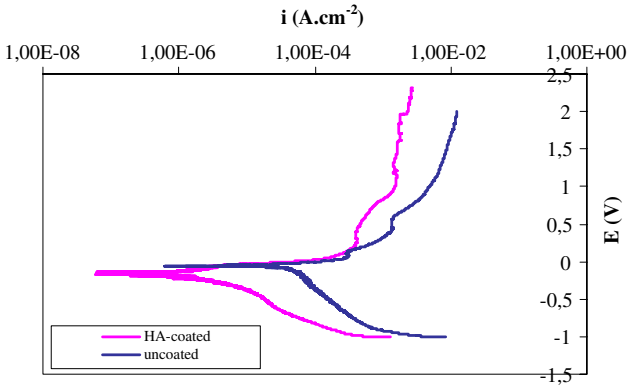

Fig. 10 Polarization curves for scaffolds in 0.9% NaCl solution at 37°C

Table 3 2-specimen average values of E_{oc}, E_{corr}, I_{corr} and R_p from polarization curves in 0.9% NaCl solution at 37°C

Scaffold	E_{oc} (mV)	E_{corr} (mV)	I_{corr} (μA)	R_p (Ω·cm^2)
Uncoated	–52 ± 1.26	–53 ± 12.62	670.0 ± 25.2	227 ± 6.81
HA-coated	–149 ± 3.16	–146 ± 6.31	39.3 ± 7.9	359 ± 3.51

Conclusions

Porous titanium scaffolds mimicking trabecular bone were successfully produced by the sacrificed polymeric sponge method. Interconnected pores in the size range of 100–600 μm corresponding to 75% porosity were obtained, resulting in structures with a compressive strength of 23.72 ± 1.12 MPa and an elastic modulus of 0.30 ± 0.003 GPa.

Sol-gel coating of pore walls with hydroxyapatite produced in vitro bioactive scaffolds, capable of further mineralization in SBF simulated plasma.

Coating also confers a greater corrosion resistance to porous titanium structures in a 0.9% NaCl solution at 37°C.

References

1. E. D. SPOERKE, N. G. MURRAY, H. LI, L. C. BRINSON, D. C. DUNAND and S. I. STUPP, *Acta Biomaterialia*. **1** (2005) 523
2. G. RYAN, A. PANDIT and D. P. APATSIDIS, *Biomaterials*. **27** (2006) 2651
3. J. -P. St-PIERRE, M. GAUTHIER, L. -P. LEFEBVRE and M. TABRIZIAN, *Biomaterials*. **26** (2005) 7319
4. J. P. LI, S. H. LI, C. A. V. BLITTERSWIJK and K. De GROOT, *J. Biomed. Mater. Res*. **73A** (2005) 223
5. C. E. WEN, Y. YAMADA, K. SHIMOJIMA, Y. CHINO, T. ASAHINA and M. MABUCHI, *J. Mater. Sci.: Mater. in Med*. **13** (2002) 397
6. S. NI, J. CHANG and L. CHOU, *J. Biomed. Mater. Res*. **76A** (2006) 196
7. J. P. LI, J. R. De WIJN, C. A. V. BLITTERSWIJK and K. De GROOT, *Biomaterials* **27** (2006) 1223

8. M. NIINOMI, *Mat. Sci. Eng*. **A243** (1998) 231
9. Z. S. RAK and J. WALTER, *J. Mater. Process. Tech.* **175** (2005) 358
10. V. A. DUBOK, *Powder Metall. M. C*. **39** (2000) 381
11. T. V. THANARAISEL and V. I. RAJESWARI, *Trends Biomater. Artif. Organs*. **18**(1) (2004) 9
12. L. L. HENCH, *J. Am. Ceram. Soc*. **81**(7) (1998) 1705–1728
13. M. TAKEMOTO, S. FUJIBAYASHI, M. NEO, J. SUZUKI, T. KOKUBO and T. NAKAMURA, *Biomaterials*. **26** (2005) 6014
14. N. OLMO, A. I. MRATÍN, A. J. SALINAS, J. TURNAY, M. VALLET-REGÍ and M. A. LIZARBE, *Biomaterials*. **24** (2003) 3383
15. H.-W. KIM, Y.-H. KOH, L.-H. LI, S. LEE and H.-E. KIM, *Biomaterials* **25** (2004) 2533
16. Y.-M. LIM, K.-S. HWANG and Y.-J. PARK, *J. Sol-Gel Sci. Techn*. **21** (2001) 123
17. F. BARRÈRE, P. LAYROLLE, C. A. V. BLITTERSWIJK and K. De GROOT, *J. Mater. Sci.: Mater. in Med*. **12** (2001) 529
18. M. NIINOMI, *Sci. Technol. Adv. Mater*. **4** (2003) 445
19. R. M. SOUTO, M. M. LAZ and R. L. REIS, *Biomaterials*. **24** (2003) 4213
20. X. LIU, P. K. CHU and C. DING, *Mat. Sci. Eng. R*. **47** (2004) 49
21. S. TAKEMOTO, M. HATTORI, M. YOSHINARI, E. KAWADA and Y. ODA, *Biomaterials*. **26** (2005) 829
22. V. GENTIL, in "Corrosão" (Livros Técnicos e Científicos Editora, Rio de Janeiro, 3ª Edição, 1996)
23. S. L. ASSIS, S. WOLYNEC and I. COSTA, *Electrochemica Acta*. **51** (2006) 1815
24. D. KRUPA, J. BASZKIEWICZ, J. KOZUBOWSKI, A. BARCZ, J. SOBCZAK, A. BILIŃSKI and B. RAJCHEL, *Vacuum* **63** (2001) 715
25. D. KRUPA, J. BASZKIEWICZ, J. W. SOBCZAK, A. BILIŃSKI and A. BARCZ, *J. Mater. Process. Tech*. **143–144** (2003) 158
26. A. BALAMURUGAN, S. KANNAN and S. RAJESWARI, *Trends Biomater. Artif. Organs*. **16**(1) (2002) 18